

Dynamic Effect in Capillary Pressure – Saturation Relationship Using Lattice Boltzmann Simulation

Guanxi Yan^{1(✉)}, Zi Li¹, Thierry Bore¹, Sergio Galindo-Torres²,
Alexander Scheuermann¹, and Ling Li²

¹ Geotechnical Engineering Centre, School of Civil Engineering,
The University of Queensland, St Lucia, QLD, Australia
g. yan@uq. edu. au

² National Centre for Groundwater Research and Training,
The University of Queensland, St Lucia, QLD, Australia

Abstract. Soil water retention curve (SWRC) as the constitutive relationship of hydro-mechanical coupling bridge of unsaturated soil has been experimentally investigated decades regarding impacts from dynamic effects in sandy soil and deformation in soft soil. However, due to inaccessibility of observation of microscale dynamic capillary behavior in geotechnical testing scale, most of the experimental methods can only provide the deviation between static SWRC and dynamic SWRC on drainage and imbibition. With the development of Computational Fluid Dynamic (CFD) simulation, several numerical methods so far can be utilized to investigate the soil water retention behavior in both micro- and macro-scale and upscaling between them, such as pore network model, Navier-Stokes integrated with Volume of Fluid and Level Set Method. Nevertheless, none of them provide a vision of interaction between fundamental fluid fractions in order to replicate the physical behavior of fluid tension from their mathematical expression. Compared to those CFD methods, Lattice Boltzmann Methods (LBM) is formulated on microscale for simulation of fluid dynamics. In addition to the interaction forces between fluid-fluid and fluid-solid phases, it fundamentally replicates the physical meaning of immiscible multiphase flow behavior in porous media. Therefore, LBM is selected to investigate the dynamic effect in soil water retention behavior in this study. The aim is to investigate the dynamic capillary pressure (soil suction in soil mechanics) varying with the saturation of each phase in a Representative Elementary Volume (REV) domain.

Keywords: Multiphase flow · Porous media · Dynamic effect · Capillary pressure · Saturation

1 Introduction

The dynamic two-phase flow seepage in porous media was theoretically extrapolated based on mass conservation (continuity equation), momentum conservation (Darcy's law) and fundamental constitutive relationships (capillary pressure/relative

permeability-saturation relations) in describing fluid-fluid retention behaviour for a Representative Elementary Volume (REV) (Buckley and Leverett 1942; Jacob 1972; Richards 1931). Therefore, the prediction of transient two-phase flow in porous media is dependent on the experimental determination of fluid-fluid retention behavior and hydraulic boundaries applied on simulating domain. Few experimental and theoretical studies from previous literatures demonstrated the velocity-dependence of capillary pressure-saturation (Abidoye and Das 2014; Barenblatt and Vinnichenko 1980; Chen 2006; Das and Mirzaei 2012; Hassanizadeh et al. 2002; Kalaydjian 1987; Mirzaei and Das 2007; O'Carroll et al. 2005; Sakaki et al. 2010; Topp et al. 1967), but those works were based on the framework of continuum mechanics without additionally understanding of multiphase physics in micro-scale. With an aim to further discover two-phase transient flow in porous media based on the microscale Computational Fluid Dynamic (CFD) simulation, the Multiphase Multicomponent Lattice Boltzmann Method (LBM) is selected as an effective approach (Galindo-Torres et al. 2013; Galindo-Torres et al. 2013; Porter et al. 2009; Schaap et al. 2007; Scheuermann et al. 2014). In comparison with other CFD methods solving Navier-Stokes equation (Ferrari 2014; Ferrari et al. 2015; Ferrari and Lunati 2013; Ferrari and Lunati 2014), Multiphase LBM own fundamental physical meanings on the fluid-fluid interface (Shan and Chen 1993).

In this study, the Shan-Chen LBM were implemented for simulating the dynamic two-phase flow in porous media and interrelationships between each pair of macroscale state variables are analyzed for further interpreting dynamic effects. According to the findings, Multiphase LBM was demonstrated as a powerful tool for investigating dynamic multiphase flow seepage. Furthermore, the research orientation for future is proposed with discussions on a few limitations in LBM model.

2 Numerical Method

2.1 Shan-Chen Multiphase Lattice Boltzmann Model

Lattice Boltzmann Method (LBM) is a method to numerically approximating the solution of Boltzmann equation by assuming statistical mechanics of microscale particles inside the single lattice node. Compared to computational fluid dynamics, which solves the problem in control volume (Navier-Stokes equation), LBM is more fundamental because it directly provides a solution from a level of particle clouds described by statistics. LBM cannot clarify the density and momentum of a single fluid particle (the fluid molecule in most case) but assign a statistical distribution between a central node and surrounding nodes to describe the probability of the density of a cloud of particles inside a specified lattice cell (Sukop 2006). A D2Q9 lattice cell is shown in Fig. 1. The microscale velocity of a single node is shown in the center of each lattice. This is like upscaling molecule scale to the specified lattice scale, and then approximate Boltzmann equation on a domain made up of these lattices, using computational iteration to determine the density and velocity of the central node of the single lattice cell for each time step. To reconstruct the particles streaming and collision mechanism in a domain, the interaction between each lattice is given by a relaxation behavior towards an equilibrium distribution of particles (Eq. (3)).

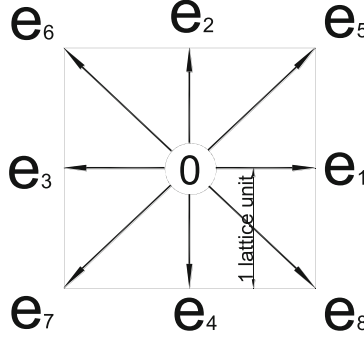


Fig. 1. D2Q9 scheme of LBM

In this experimental study, LBM is just taken as a numerical experiment to explore the dynamic effect. The D2Q9 SCLBM engine is available in Mechsys (Multi-physics Simulation Library, developed by Dr. Sergio Galindo Torres at School of Civil Engineering, the University of Queensland). The construction of this Shan-Chen LBM (SCLBM) engine is listed in Table 1. The explanation of LBM in details can be sourced from Sukop (2006).

Equations (1)–(4) give the standard LBM using BGK equilibrium distribution function. Shan-Chen LBM added inter-particle pseudo forces (Eq. (5)), multiphase repulsive force (Eq. (7)) and particle-solid interaction force (Eq. (8)) to simulate compressibility of each fluid phase and interface (Shan and Chen 1993). Due to introducing these lattice interaction forces, velocity for equilibrium distribution function has to be locally averaged using Eq. (9). In the single component multiphase system, there is only in need of interparticle attractive force (Eq. (5)). For the multi-component, multiphase system, Eq. (5) is modified to Eq. (8) to conduct attraction between wetting phase and solid particles and repulsion between non-wetting phase and solid particles. When the lattice cell contains solid nodes on one side of four edges, to generate the solid adsorption behavior, an imbalance force between fluid-fluid and fluid-solid is given by setting function distributions to unity instead of density.

Table 1. The construction of D2Q9 Shan-Chen LBM simulation engine

D2Q9 Cell	<p>Lattice Fluid Density: $\rho = \sum_{i=0}^8 f_i$ (1)</p> <p>Lattice Fluid Velocity: $\mathbf{u} = \frac{\sum_{i=0}^8 f_i \mathbf{e}_i}{\rho}$ (2)</p>
Governing Equation	$\underbrace{f_i(\mathbf{x} + \mathbf{e}_i \Delta t, t + \Delta t) - f_i(\mathbf{x}, t)}_{\text{Streaming}} = \underbrace{\left[\underbrace{w_i \rho(\mathbf{x}) \left(1 + 3 \frac{\mathbf{e}_i \cdot \mathbf{u}}{C} + 4.5 \frac{(\mathbf{e}_i \cdot \mathbf{u})^2}{C^4} - 1.5 \frac{\mathbf{u}^2}{C^2} \right)}_{\text{Bhatnagar–Gross–Krook (BGK) approximation of } f_i^{eq}} - f_i(\mathbf{x}, t) \right]}_{\substack{\text{Collision} \\ \underbrace{\frac{3}{c_s} + \frac{1}{2}}_{\text{Relaxation time} \geq 0.5}}} \quad (3)$
Body Force Equation	Newton Second Law: $\mathbf{u}^{eq} = \mathbf{u} + \frac{\tau \mathbf{F}}{\rho}$ (4)
Particles interaction Force	$F_a = -G_a \psi_j(\mathbf{x}, t) \sum_{i=1}^8 w_i \psi_j(\mathbf{x} + \mathbf{e}_i \Delta t, t) \mathbf{e}_i$ (5)
LBM EOS	$P = \frac{\rho}{3} + \frac{G}{6} \psi_0^2 \exp\left(\frac{-2\rho_0}{\rho}\right)$ (6)
Immiscible Multiphase Equations	<p>Immiscible fluids repulsive force: $F_r = -G_r \rho_j(\mathbf{x}, t) \sum_{i=1}^8 w_i \rho_j(\mathbf{x} + \mathbf{e}_i \Delta t, t) \mathbf{e}_i$ (7)</p> <p>Solid-Fluids interaction force: $F_s = -G_s \psi_j(\mathbf{x}, t) \sum_{i=1}^8 w_i s(\mathbf{x} + \mathbf{e}_i \Delta t, t) \mathbf{e}_i$ (8)</p>
Correction Equation for f_i^{eq}	<p>Velocity Correction: $\mathbf{u} = \frac{\sum_{\sigma} \frac{1}{\tau \sigma} \sum_{i=0}^8 f_i^{\sigma} \mathbf{e}_i}{\sum_{\sigma} \frac{\rho_{\sigma}}{\tau \sigma}}$ (9)</p> <p>Density for each phase: $\rho_{\sigma} = \sum_{i=0}^8 f_i^{\sigma}$ (10)</p>
Pressure of single cell	$P(x) = \frac{\rho_j(x) + \rho_f(x) + G_r \rho_j(x) \rho_f(x)}{3}$ (11)
Young-Laplace Equation for SCLBM	<p>Capillary pressure: $P_c = P_f - P_j = \frac{2\sigma_s}{R}$ (12)</p> <p>Contact angle: $\cos \theta = \frac{G'_s - G'_s}{G_r}$ (13)</p>

where f_i = distribution function for direction i projecting from central node of single lattice, e_i = discretised velocity shooting from central node to surrounding nodes of single lattice, f_i^{eq} = equilibrium distribution function, \mathbf{x} = the position vector of single node, t = time, τ = relaxation time (better close to 1), $C = \Delta t / \Delta x$ ($\Delta t = 1$ ts, $\Delta x = 1$ lu, $v = \mu / \rho$ kinematic viscosity, c_s = speed of sound of lattice ($C/3^{0.5}$), u^{eq} = macroscale fluid Velocity in equilibrium, F_a = body force (it could be Gravity only if there is no other action), G_a = attractive intensity between fluid particles of single phase, ψ_j = interaction potential of phase j , w_j = weight factor of phase j for each node in single cell ($w_0 = 4/9$, $w_{1-4} = 1/9$, $w_{5-8} = 1/36$), s = a 'switch' value usually to be density but is switched to 1 if zero velocity solid boundary are encountered, ψ_0 = constant initial interaction potential, ρ_0 = constant initial macroscale density, F_r = immiscible phase repulsive force, G_r = two phase repulsive intensity (positive value), F_s = fluid-solid interaction force (attraction for wetting phase j and repulsion for non-wetting phase j'), G_s = fluid-solid attractive/repulsive intensity, ρ_j = macroscale density of wetting phase j , $\rho_{j'}$ = macroscale density of non-wetting phase j' , σ_s = surface tension, θ = contact angle, G'_s = wetting phase fluid-solid attractive intensity (negative value), $G'^s_{j'}$ = non-wetting phase fluid-solid repulsive intensity (positive value).

2.2 Simulation Setup

For simulating two-phase flow in 2D porous media, a package of perfect circular disk is filled into a 500×500 square of lattice 2D LBM domain as shown in Fig. 2. The cyan background is the void space, where the two-phase flow is percolating through the colorful disks representing the granular soil particles in this domain. This setup aims to replicate the phase displacement phenomenon, so the right and left boundary conditions are fixed to solid as same as the outline of each grain using bounce back boundary conditions in Sukop and Thorne (2006)

$$f_i = f_{-i} \quad (14)$$

where $-i$ represents the distribution function reverse its direction after a fluid collision with a solid boundary. The top and bottom boundary conditions are directly controlled by density difference without any buffer zone, which represents pressure difference using LBM EOS transformation (Eq. (11)). Wetting or non-wetting phase fluid is fully filled into void space as the initial condition for drainage or imbibition simulation.

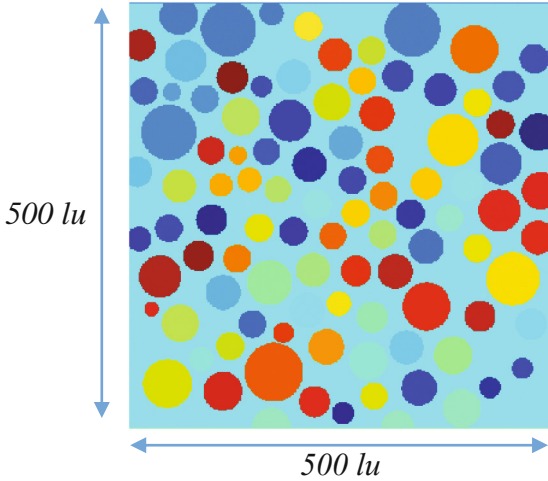


Fig. 2. A package of circular disk in $500 \times 500 \text{ lu}^2$ 2D lattice domain

Grain Size Distribution (GSD) is measured using the Image Toolbox built in MATLAB[®] R2014b. Pore Size Distribution (PSD) is measured using the image processing algorithm developed by Rabbani et al. (2014). The GSD and PSD of virtual soil are shown in Fig. 3. According to Fig. 3, the PSD is wider than GSD, and mean pore size is larger than the mean grain size, so the packing condition is not identical to natural soil but similar to glass beads package with a lot of interconnected pore channels.

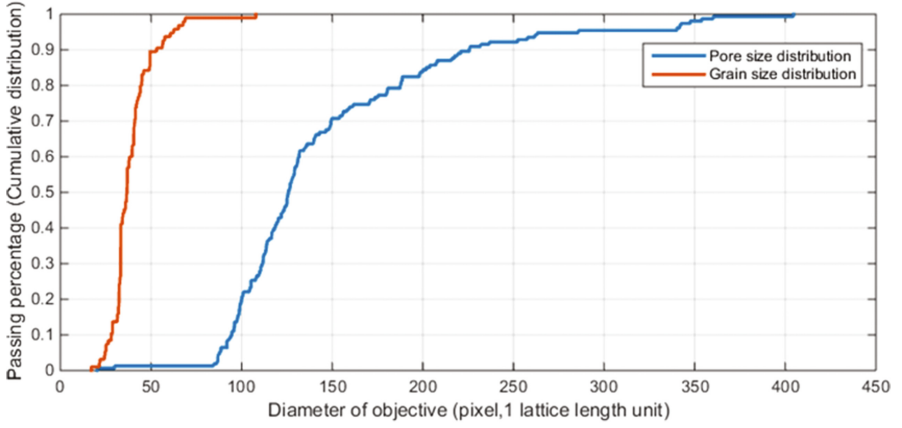


Fig. 3. Pore size distribution and Grain size distribution of virtual grains in 2D LBM simulation

The parameters for this simulation setup is given in Table 2. According to this set of parameters, the lattice surface tension is determined at $0.1818 \mu u / \Delta t s^2$ using bubble simulation, and the contact angle is set to zero calculated by Eq. (13). Once the simulation initiates, non-wetting phase or wetting phase drives into void space by density difference boundary between top and bottom, until there is an equilibrium achieved between such density difference and interfacial meniscus. In this state, the single data point on static Capillary Pressure – Saturation (P_c-S_w) is derived. By applying density difference from zero to a value that can drain each phase out of the void domain, various capillary equilibrium condition can be produced to the corresponding saturation of wetting phase measured by counting pixels occupied by wetting phase fluid.

Table 2. Lattice-scaled parameter values used in numerical experiment

Lattice-scaled Parameters	Value
Wetting phase fluid density	2.0
Non-wetting phase fluid density	2.0
Dynamic viscosity of wetting phase fluid	0.16
Dynamic viscosity of non-wetting phase fluid	0.16
Lattice unit length	1.0
Lattice time step	1.0
Two phase repulsive intensity	1.0
Wetting fluid attractive intensity	-0.5
Non-wetting fluid attractive intensity	0.5
Gross simulation time	500000
Time interval	5000
Density difference/Initial density	0% – 80%
Initial density for two-phase fluids	2.0
Infinitesimal density for each other phase for mixing	0.0001

As for post data analysis, the results of the simulation are given in four arrays: wetting phase density, wetting phase velocity, non-wetting phase density, and non-wetting phase velocity. The macroscale pressure of each fluid phase is determined using Eq. (11) in consideration of a small amount of the other phase mixing inside (Galindo-Torres et al. 2013). Finally, the capillary pressure (P_c) can be given by the difference between pressures of two mixing areas (two fluid phases) using Eq. (12). The saturation of wetting fluid phase (S_w) can be determined by counting the lattice nodes (Eq. (15)) when local density is larger than half of initial density. This density threshold rule has been applied by Porter et al. (2009) and Galindo-Torres et al. (2013). As for the measurement of the specific interfacial area (a_{nw}), the area of each fluid phase and solid phase can be given by counting the pixel occupied by interfaces between each pair of phases. Finally, the specific interfacial area is calculated using Eq. (16). With known capillary pressure, saturation for both two-phase fluids and interfacial area of the two-phase meniscus on the end of each time interval, the static P_c - S_w - a_{nw} or dynamic P_c - S_w - a_{nw} can be extracted from equilibrium approached and transient flow conditions (Table 3).

Table 3. Upscaling post analysis for determining the microscale variables

Macroscale state variables (REV scale)	Upscaling equations
Saturation (S_w)	wetting phase: $S_w = \frac{\sum_{i=1}^{N_w} A_{i,w}}{\sum_{i=1}^{n_T} A_i}$ (15)
Interfacial area (A_{nw})	Specific interfacial area: $a_{nw} = \frac{\sum_{i=1}^{N_w} A_{i,w} + \sum_{i=1}^{N_{nw}} A_{i,nw} - \sum_{i=1}^{n_{nw}} A_{i,s}}{2 \sum_{i=1}^{n_T} A_i}$ (16)

3 Result and Analysis

3.1 Performance of SC-LBM Simulation for One-Step in/Outflow

According to Table 4, there is an observation that with the pressure difference increase between the top and bottom boundary, more wetting phase is pushed out the beads package, and more non-wetting phase invaded the domain. When the density difference on two boundaries achieves 0.4 mu/lu^2 , a preferential path is generated in the center of virtual soil. The wetting phase fluid is separated into two portions on two corners of bottom separately. In this simulation, to reduce computational effort, the initial density and viscosity ratio are both set at one as listed in Table 2. Therefore, such a preferential path is not caused by different flow patterns, but geometrical determined, where the larger pore throat, where the non-wetting phase breaks through the entry pressure first.

According to the Table 5, the imbibition process shows more preferential paths on the left side of the domain because the pore throats on the left are smaller than the right

Table 4. Visualization of 2D LBM simulation of drainage

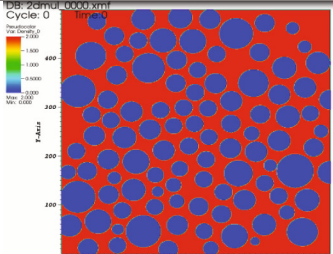
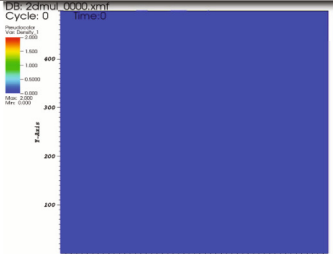
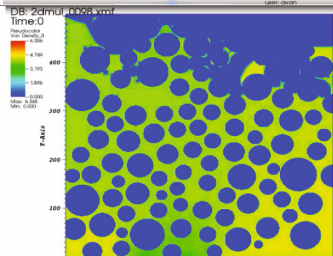
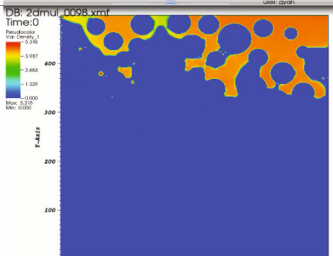
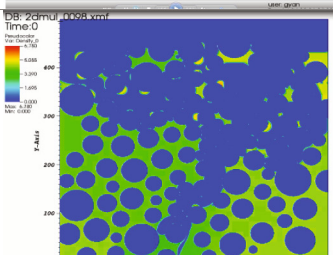
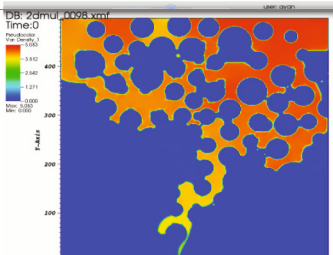
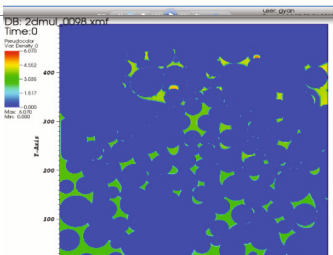
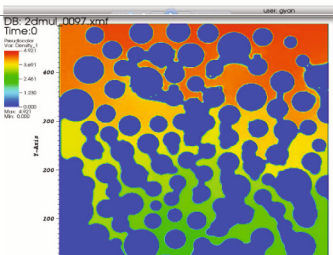
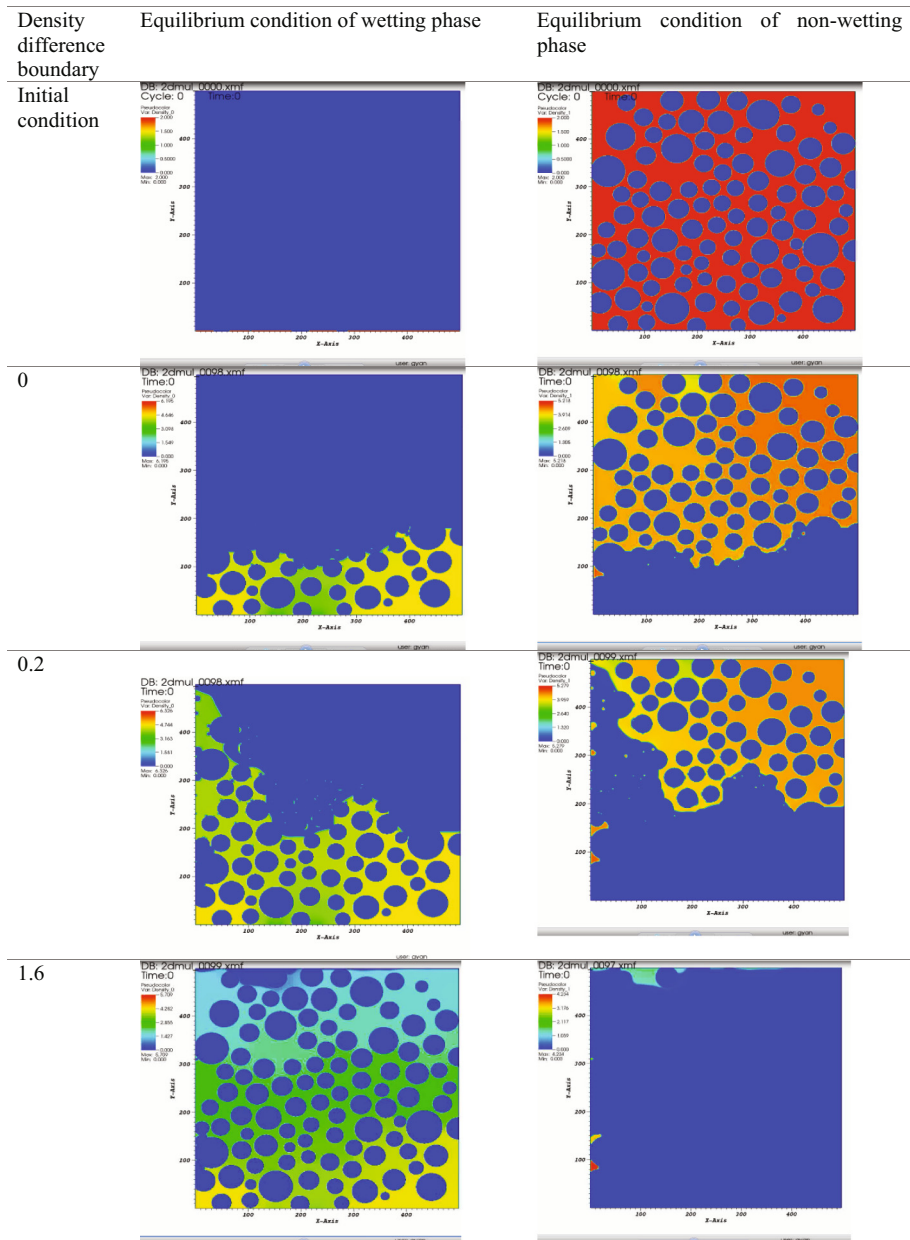
Density difference boundary	Equilibrium condition of wetting phase	Equilibrium condition of non-wetting phase
Initial condition		
0		
0.4		
1.2		

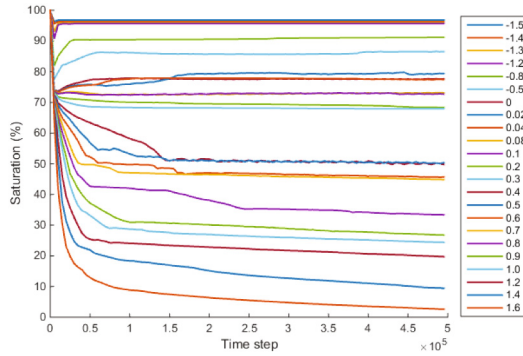
Table 5. Visualization of 2D LBM simulation of imbibition



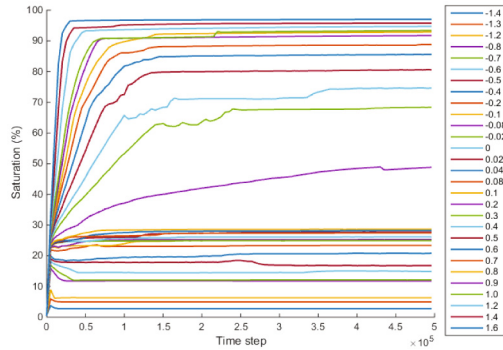
side. Also, a small amount of wetting phase trapping and non-wetting phase trapping can be found. However, this trapping is only a little in the domain. When the final equilibrium achieved, most of the trapping phase slowly evaporates, causing a slight decrease of each trapping phase fluid. This simulating performance is consistent with Schaap et al. (2007). Schaap et al. (2007) claimed their confidence on their results having such issues. Here, we follow their recommendations on neglecting the disappearance of phase trapping. The visualization in Tables 4 and 5 demonstrates that the SCLBM physically replicates capillary flow in a granular porous media, and the observation is consistent with two-phase displacement in natural porous media.

3.2 Dynamic Effects in Capillary Pressure-Saturation Curves

The static and dynamic P_c-S_w simulated using SCLBM are plotted in Fig. 5(a). Each data point is taken for plotting static P_c-S_w after equilibrium achievement. The equilibrium of static P_c-S_w is ensured by checking the S_w varying with lattice time step shown in Fig. 4. After 2×10^5 time steps, the equilibrium is approached already with a



(a)



(b)

Fig. 4. Historical logging of Saturation for various density boundary conditions listed in legend: (a) Drainage, (b) Imbibition

slight fluctuation caused by numerical artifact on meniscus instability of wetting front. The dynamic responses under transient flow conditions are more significantly within a first 0.5×10^5 time step. Within this period, the dynamic P_c - S_w - a_{nw} can be plotted, as can be checked from Fig. 5(c).

Except for some anomaly for bubble point and residual trapping saturation of drainage P_c - S_w , the results shown in Fig. 5 replicate the primary static drainage and imbibition P_c - S_w highlighted in yellow zone in Fig. 5, and the area of dynamic P_c - S_w highlighted in dark blue zone in Fig. 5. Also, having the plot of P_c - S_w corresponding to each time frame of simulation, the dynamic P_c - S_w can be checked through a simulation

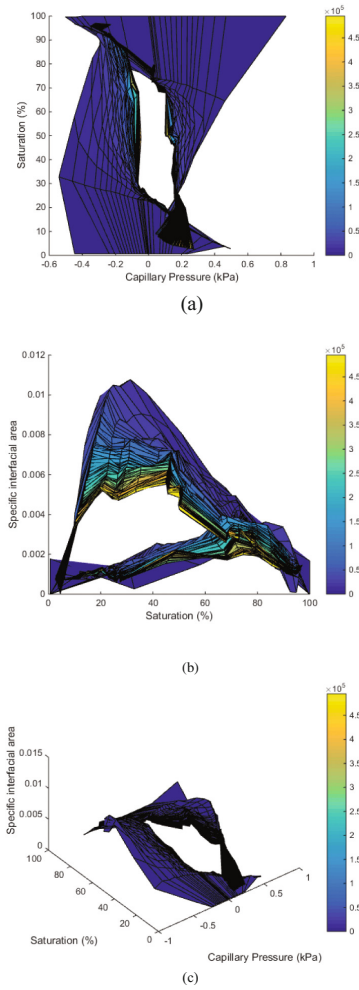


Fig. 5. Dynamic P_c - S_w - a_{nw} relationship with contour color bar marking the time step: (a) the projection of 3D contour plot of P_c - S_w - a_{nw} on 2D P_c - S_w plane, (b) the projection of 3D contour plot of P_c - S_w - a_{nw} on 2D S_w - a_{nw} plane, (c) Dynamic P_c - S_w - a_{nw} relationship

of transient two-phase displacement in the virtual soil. This is a demonstration of dynamic capillary effect in P_c-S_w for a transient two-phase seepage, which is missed in our conventional theory just requiring achievement of equilibrium on every time step instantaneously.

These results are the first effort on studying dynamic multiphase flow in porous media using 2D SCLBM. Although the model setup is simple, it is still a good beginning for applying SCLBM to investigate dynamic effects in immiscible fluid retention behavior under transient flow conditions. Due to the dimensional constraints, the simulation result temporarily can only be seen as a straightforward proof. The 2D setup leads to less phase trapping, and large pore throats as shown in Tables 4 and 5 additionally result in low capillary entry pressure or even positive pore pressure for imbibition process as shown in Fig. 5(a). In the future, quasi-2D and 3D setup are worth to be implemented for a better replication of physical testing conditions.

3.3 Dynamic Effects in Capillary Pressure-Saturation-Specific Interfacial Area

The other interesting theoretical framework in the advanced theory of multiphase flow in porous media is the uniqueness of $P_c-S_w-a_{nw}$ constitutive surface proposed by Hassanizadeh and Gray (1993b). Porter et al. (2009) confirmed the uniqueness of the static $P_c-S_w-a_{nw}$ surface using 3D SCLBM. However, there is no any information about the dynamic effect for this constitutive surface under transient flow using SCLBM. Hence, the 2D SCLBM is applied here to discover the uniqueness of surface under transient condition. Karadimitriou et al. (2014) experimentally investigated this constitutive surface under transient condition using an elongated PDMS micromodel, and find that this surface is not unique under transient flow condition. Also, it is Capillary number dependent, which means that it depends on seepage velocity. Joekar-Niasar et al. (2010) also studied this surface under transient condition using numerical dynamic pore network model and concluded that due to the each phase fluid losing continuity in a transient condition, there is a significant discrepancy between equilibrium and nonequilibrium constitutive surface. For this numerical experiment, the evolution of these three state variables is plotted in Fig. 5.

From Fig. 5(b), there is a clear temporal evolution of wetting phase saturation-interfacial area. Checking through the color bar representing the time step, it is straightforward to find that there is less variation of saturation-interfacial area relationship after 1×10^5 time steps. Beforehand, there is a different saturation-interfacial area plot within each time step. In Fig. 5(b), the curves for drainage is located on the upper side while the curves for imbibition is located downside. The saturation-interfacial area relationship follows different paths for hydraulic loading history. This also replicates the physical phenomenon that meniscus area is pulled larger for drying than for wetting process in which the curvature of the meniscus alleviated by fluid inertial (Hoffman 1983). It is also an explanation that there is no relationship between the dynamic contact angle of the meniscus and static hysteresis of SWRC because the dynamic contact angle contributes to the capillary pressure difference between dynamic and static capillary pressure (Hassanizadeh and Gray 1993a), but the data points of static hysteresis SWRC is taken on equilibrium state.

The Fig. 5(c) shows the variation of the 3D capillary pressure-saturation-interfacial area with time forwarding to the next equilibrium state for each density difference boundary condition. The temporal evolution of imbibition is on the left side while the other temporal evolution of drainage is on the right side. As can be seen from the color bar of temporal evolution in Fig. 5(c), it is evident that the equilibrium can only be achieved when there is no variation of the specific interfacial area. Most of the dynamic variation of capillary pressure and the interfacial area is located within $0-1 \times 10^5$ time steps. Only within this time scale, there is significant saturation varying with time, indicating that there is real flux seepage through this assumed Darcy scale REV. Once the equilibrium achieved, the static SWRC can be plotted, but there is no flow at all. When the dynamic process is ongoing from one state to next state, the capillary pressure-saturation-interfacial area is continuously changing with time steps. There is no any uniqueness of SWRC and the 3D constitutive surface for the evolution of the state.

4 Conclusion and Reflection

In this study, the Shan-Chen Lattice Boltzmann simulation is conducted to model two-phase flow displacement in a granular porous media. According to the simulation performance, it can conclude that SCLBM is a powerful tool to investigate multiphase hydrodynamic seepage problems for unsaturated flow in the vadose zone and oil reservoir enhancement. The results manifest that the SCLBM can replicate the dynamic effects in fluid-fluid retention behavior. Also, the capillary pressure-saturation relationship shows a transitional behavior between initial states and next equilibrium state under transient flow conditions. However, according to the conventional theory, the transition from one state to the next is assumed to follow the capillary pressure-saturation curve only in the static state. Also, the larger the density boundary (pressure boundary of LBM) applied, the larger the dynamic capillary pressure response and larger interfacial area variation appear during a transient process. These findings might lead to a further question on how the effective hydraulic conductivity can be evaluated based on the static P_c-S_w using any empirical and statistical Hydraulic Conductivity Function (HCF) models. According to the nonlinear diffusion theory, which is the mathematical form of Richards' equation, the temporal evolution of the volumetric water content should be equal to the divergence of the flux in 3D space. If the flux for each dimension cannot be approximated using the hydraulic conductivity predicted by static P_c-S_w , the purpose of using such theory somehow becomes questionable. More interestingly, so far the HCF models are all correlated to only the static drainage P_c-S_w by adopting phase fraction network assumptions. Under the transient flow condition, there is no guarantee for this continuous phase flowing through the fraction they occupied. The dynamic P_c-S_w is an indication of the dynamic response of two-phase displacement in porous media. The application on the estimation of seepage flux so far has not been investigated yet. Each dynamic P_c-S_w only exists within evolution, and finally, return to static one. Incorporating dynamic relationships into Richard's equation, therefore, seems vague on explaining the physical meaning of HCF. For further investigating the dynamic multiphase flow, flow governing equation

in regards to relative permeability concept for calculating two-phase seepage flux should be further studied using SCLBM.

Acknowledgements. The first author wants to acknowledge the support from the University of Queensland International Scholarship (UQI). The simulations were implemented using the Mechsys open source library on the Macondo high-performance cluster, currently merged into Goliath supercluster, at the University of Queensland.

References

- Abidoye, L.K., Das, D.B.: Scale dependent dynamic capillary pressure effect for two-phase flow in porous media. *Adv. Water Resour.* **74**, 212–230 (2014)
- Barenblatt, G.I., Vinnichenko, A.: Non-equilibrium seepage of immiscible fluids. *Adv. Mech.* **3**(3), 35–50 (1980)
- Buckley, S.E., Leverett, M.: Mechanism of fluid displacement in sands, 146(01), 107–116 (1942)
- Chen, L.: Hysteresis and dynamic effects in the relationship between capillary pressure, saturation, and air-water interfacial area in porous media (2006)
- Das, D.B., Mirzaei, M.: Dynamic effects in capillary pressure relationships for two-phase flow in porous media: Experiments and numerical analyses. *AIChE J.* **58**(12), 3891–3903 (2012)
- Ferrari, A.: Pore-scale modeling of two-phase flow instabilities in porous media. University of Torino (Italy) (2014)
- Ferrari, A., Jimenez-Martinez, J., Borgne, T.L., Méheust, Y., Lunati, I.: Challenges in modeling unstable two-phase flow experiments in porous micromodels. *Water Resour. Res.* **51**(3), 1381–1400 (2015)
- Ferrari, A., Lunati, I.: Direct numerical simulations of interface dynamics to link capillary pressure and total surface energy. *Adv. Water Resour.* **57**, 19–31 (2013)
- Ferrari, A., Lunati, I.: Inertial effects during irreversible meniscus reconfiguration in angular pores. *Adv. Water Resour.* **74**, 1–13 (2014)
- Galindo-Torres, S., Scheuermann, A., Li, L., Pedroso, D., Williams, D.: A lattice boltzmann model for studying transient effects during imbibition–drainage cycles in unsaturated soils. *Comput. Phys. Commun.* **184**(4), 1086–1093 (2013)
- Galindo-Torres, S., Scheuermann, A., Pedroso, D., Li, L.: Effect of boundary conditions on measured water retention behavior within soils. In: AGU Fall Meeting Abstracts, p. 1516 (2013)
- Hassanizadeh, S.M., Celia, M.A., Dahle, H.K.: Dynamic effect in the capillary pressure–saturation relationship and its impacts on unsaturated flow. *Vadose Zone J.* **1**(1), 38–57 (2002)
- Hassanizadeh, S.M., Gray, W.G.: Thermodynamic basis of capillary pressure in porous media. *Water Resour. Res.* **29**(10), 3389–3405 (1993a)
- Hassanizadeh, S.M., Gray, W.G.: Toward an improved description of the physics of two-phase flow. *Adv. Water Resour.* **16**(1), 53–67 (1993b)
- Hoffman, R.L.: A study of the advancing interface: II. Theoretical prediction of the dynamic contact angle in liquid-gas systems. *J. Colloid Interface Sci.* **94**(2), 470–486 (1983)
- Jacob, B.: *Dynamics of Fluids in Porous Media*. Dover Publications, New York (1972)
- Kalaydjian, F.: A macroscopic description of multiphase flow in porous media involving spacetime evolution of fluid/fluid interface. *Transp. Porous Media* **2**(6), 537–552 (1987)

- Karadimitriou, N., Hassanizadeh, S., Joekar-Niasar, V., Kleingeld, P.: Micromodel study of two-phase flow under transient conditions: Quantifying effects of specific interfacial area. *Water Resour. Res.* **50**(10), 8125–8140 (2014)
- Mirzaei, M., Das, D.B.: Dynamic effects in capillary pressure–saturation relationships for two-phase flow in 3D porous media: Implications of micro-heterogeneities. *Chem. Eng. Sci.* **62**(7), 1927–1947 (2007)
- O’Carroll, D.M., Phelan, T.J., Abriola, L.M.: Exploring dynamic effects in capillary pressure in multistep outflow experiments 41(11) (2005)
- Porter, M.L., Schaap, M.G., Wildenschild, D.: Lattice-Boltzmann simulations of the capillary pressure–saturation–interfacial area relationship for porous media. *Adv. Water Resour.* **32** (11), 1632–1640 (2009)
- Rabbani, A., Jamshidi, S., Salehi, S.: An automated simple algorithm for realistic pore network extraction from micro-tomography images. *J. Petrol. Sci. Eng.* **123**, 164–171 (2014)
- Richards, L.A.: Capillary conduction of liquids through porous mediums. *J. Appl. Phys.* **1**(5), 318–333 (1931)
- Sakaki, T., O’Carroll, D.M., Illangasekare, T.H.: Direct quantification of dynamic effects in capillary pressure for drainage–wetting cycles. *Vadose Zone J.* **9**(2), 424–437 (2010)
- Schaap, M.G., Porter, M.L., Christensen, B.S., Wildenschild, D.: Comparison of pressure–saturation characteristics derived from computed tomography and lattice Boltzmann simulations 43(12) (2007)
- Scheuermann, A., Galindo-Torres, S., Pedroso, D., Williams, D., Li, L.: Dynamics of water movements with reversals in unsaturated soils. In: 6th International Conference on Unsaturated Soils, UNSAT 2014, pp. 1053–1059 (2014)
- Shan, X., Chen, H.: Lattice Boltzmann model for simulating flows with multiple phases and components 47(3), 1815 (1993)
- Sukop, M., Thorne, D.T.: *Lattice Boltzmann Modeling*. Springer, Heidelberg (2006)
- Topp, G., Klute, A., Peters, D.: Comparison of water content–pressure head data obtained by equilibrium steady-state and unsteady-state methods. *Soil Sci. Soc. Am. J.* **31**(3), 312–314 (1967)

Proceedings of the 2nd International Symposium on
Asia Urban GeoEngineering

Chen, R.; Zheng, G.; Ou, C. (Eds.)

2018, XVIII, 697 p. 432 illus., Hardcover

ISBN: 978-981-10-6631-3